Applied Catalysis B: Environmental 209 (2017) 110–117

Contents lists available at ScienceDirect

Applied Catalysis B: Environmental

journal homepage: www.elsevier.com/locate/apcatb

Enhanced photoelectrochemical properties of ZnO/ZnSe/CdSe/$Cu_{2-x}Se$ core–shell nanowire arrays fabricated by ion-replacement method

Yuanlu Chen [a], Lijuan Wang [a], Wenzhong Wang [b,*], Maosheng Cao [a,*]

[a] School of Materials Science and Engineering, Beijing Institute of Technology, Beijing, 100081, China
[b] School of Science, Minzu University of China, Beijing, 100081, China

ARTICLE INFO

Article history:
Received 12 December 2016
Received in revised form 2 February 2017
Accepted 12 February 2017
Available online 20 February 2017

Keywords:
ZnO/ZnSe/CdSe/$Cu_{2-x}Se$ core–shell nanowire arrays
p-n Junction
PEC performance

ABSTRACT

The core-shell structures are designed to take advantages of each material to improve the photoelectrochemical (PEC) performance. Here we report a facile ion-replacement strategy for fabricating ZnO/ZnSe/CdSe/$Cu_{2-x}Se$ core–shell nanowire arrays grown on Fluorine-doped tin oxide (FTO) glass under hydrothermal conditions. Under illumination with AM 1.5G, the designed ZnO/ZnSe/CdSe/$Cu_{2-x}Se$ core–shell nanowire arrays exhibit superior PEC performance with the highest photocurrent density of 20.57 mA/cm^2, which is 29.4 times higher than that of the ZnO nanowire arrays at 0 V versus Ag/AgCl, and achieve the incident photon conversion efficiency (IPCE) of 87.6% at 410 nm without applying bias potential. The superior PEC performance of the ZnO/ZnSe/CdSe/$Cu_{2-x}Se$ core–shell nanowire arrays results from the synergistic effects of each material. Vertical aligned ZnO hexagonal prisms provided large specific surface area and electron access along the axial direction. ZnSe layer further extended specific surface area and the range of light absorption. CdSe layer enhanced the visible light absorption vastly and fully utilized the incident light. P-type $Cu_{2-x}Se$ layer produced p-n junctions, which could not only prevent the recombination, but also promote the separation and transmission of photo-generated electron-hole pairs. The synergistic action of each component in ZnO/ZnSe/CdSe/$Cu_{2-x}Se$ core–shell nanowire arrays led an outstanding PEC performance. The synthetic strategy achieved in this work can have promising applications for designing highly efficient electrodes of other materials for water splitting.

1. Introduction

The energy problem, especially the oil source, is becoming more and more serious. It is well known that solar energy is the ideal energy source for its unexhausted and environmentally friendly. However, there are technical problems waiting to be solved for the collection, conversion, storage and utilization of solar energy. Hydrogen energy is an attractive medium to convert and store solar energy since it is clean and efficient. The conversion from solar energy to chemical energy (e.g. hydrogen energy) via semiconductor photocatalyst has been one of the most important scientific challenges in recent years. Thus, PEC and photocatalysis have the potential to generate hydrogen from solar energy. PEC performance and photocatalysis activity have been widely studied in different semiconductor materials [1–8]. However, at the present the energy conversion efficiency couldn't achieve the demands of industrialization production. Semiconductors with single component are always subject to the intrinsic property of the materials. As a result, the PEC performance and photocatalysis activity are often unsatisfactory. It is well known that metallic oxide semiconductor ZnO [9–11] and TiO_2 [12–14] are common photocatalyst due to their stability, extensive sources and low cost. Nevertheless they are subject to the wide band gap, which limited the activities in visible light region. The energy in UV light region accounts for less than 5% of solar energy. Besides, metal selenide semiconductors such as ZnSe [15,16] and CdSe [17,18] with narrow-bandgap have outstanding visible light absorption but suffer from photostability. Thus an ideal PEC functional material should have both superior light absorption and high photostability. In this way, manufacture of heterojunctions between the interfaces of the ZnO and metal selenide semiconductors such as ZnSe and CdSe is a promising strategy for fabricating ideal PEC functional material because it can both extend the light absorption range and improve the stability as well as electron mobility.

* Corresponding authors.
E-mail addresses: wzhwangmuc@163.com (W. Wang), caomaosheng@bit.edu.cn (M. Cao).

http://dx.doi.org/10.1016/j.apcatb.2017.02.049
0926-3373/

ZnO is a kind of wide-bandgap semiconductor (3.3 eV) [19] with large exciton binding energy (60 meV) [20]. It has been widely investigated as the suitable succedaneum of TiO_2 because of its chemical stability, hypotoxicity and low refractive index. Well-aligned vertical arrays of ZnO nanowire endow effective electron access along the axial direction [21]. Moreover, the rice-field-liked nanowire arrays enhance the specific surface area, which improves the light absorption. The advantages above make ZnO nanowire arrays to be one of the appropriate choices for anode material of efficient PEC batteries. However the weakness of ZnO has restricted its application, such as the light absorption limited in UV range and the short lifetime of charge carriers, which confine the photoelectric conversion efficiency.

It has been demonstrated that modifying ZnO nanowire arrays with narrow-bandgap semiconductors is an efficient method to expand the visible light absorption region. The efficiency of the separation and transportation of charge carriers would also get benefits from the manufacture of the heterostructures. ZnSe is a suitable choice to build the type-II heterojunctions with ZnO since it has a band gap of 2.7 eV [22], which is slightly less wider than that of ZnO. CdSe layer coated over ZnO/ZnSe nanowire arrays can further promote the range of light absorption benefited by the narrow band gap of 1.7 eV [23], however the photocorrosion in aqueous solution under illumination obstructs the application [24]. What's worse, there is slow transmission for photo-generated holes between electrolyte and CdSe. Electrolyte added with hole scavenger such as Na_2S and Na_2SO_3 can stabilize photocatalyst during the PEC test [25], but the actual effect is still not satisfactory. Surface states and defects can be passivated by the establishment of p-n junctions that can both prevent the recombination and accelerate the separation and transmission of photo-generated charge carriers [26]. $Cu_{2-x}Se$ layer constructed over the surface of ZnO/ZnSe/CdSe nanowire arrays is competent as a group of narrow-bandgap p-type semiconductors.

In this work, ZnO/ZnSe/CdSe/Cu_{2-x}Se core-shell nanowire arrays have been synthesized by a series of consecutive ion-replacement reactions under hydrothermal conditions. The well-aligned nanowire arrays gain large specific surface area, which are accompanied by excellent light absorption. In addition, the matched band gap structures are beneficial to the separation and transmission of photo-induced charge carriers. Moreover, the heterojunctions between the interfaces further advance the photoelectric conversion efficiency. ZnO/ZnSe/CdSe/Cu_{2-x}Se core-shell nanowire arrays take advantages of each component in the composite structure with the aim of preeminent PEC performance.

2. Experiment section

2.1. Materials

All the chemicals in this work were of analytical grade. Zinc acetate ($Zn(OAc)_2$), hexamethylenetetramine (HMTA), cadmium nitrate tetrahydrate ($Cd(NO_3)_2{\cdot}4H_2O$) and copper (II) nitrate trihydrate ($Cu(NO_3)_2{\cdot}3H_2O$) were purchased from Sinopharm Chemical Reagent Co. Ltd (Shanghai, China), while zinc nitrate hexahydrate ($Zn(NO_3)_2{\cdot}6H_2O$), selenium powder (Se, −200 mesh, 99.999%) and sodium borohydride ($NaBH_4$) were purchased from Beijing Chemical Works (Beijing, China), Alfa Aesar, USA and HNC Technology Development Co. Ltd (Tianjin, China), respectively. These chemicals were used as received without any further purification. Deionized water with resistivity higher than 18.4 MΩ/cm was obtained from a water purification system Mini-Qx-3000 (Qunxian, China). FTO glass (bought from Nippon Sheet Glass Company, Japan) was incised into 1.5 cm × 3 cm per piece.

2.2. Synthesis of ZnO/ZnSe/CdSe/Cu_{2-x}Se nanowire arrays

The synthesis process was modified from the reports of Lee et al. [27] and Zhang et al. [28]. As illustrated in Fig. 1, ZnO nanowire arrays were firstly grown on FTO glass by a hydrothermal process. Subsequently, a series of consecutive ion-replacement reactions via hydrothermal method occurred to fabricate ZnO/ZnSe, ZnO/CdSe, ZnO/ZnSe/CdSe and ZnO/ZnSe/CdSe/Cu_{2-x}Se samples.

ZnO nanowire arrays were prepared by following processes. Firstly, FTO glass was cleaned with acetone, ethyl alcohol and deionized water sequentially by an ultrasonic cleaner KQ5200DE (Shumei, China). Then 5 mM ethanol solution of zinc acetate was spin-coated onto the conductive side of the cleaned FTO glass by a spin-coater KW-4A (SiYouYen, China), while the spin-coating area was 1.5 cm × 2 cm. This process was repeated 5 times to coat appropriate zinc acetate uniformly over the FTO glass, followed by annealing to form the seed layer in air at 350 °C for 20 min in a tube-furnace GSL-1100X (KmtFurnace, China). ZnO nanowire arrays were grown by immersing the prepared seed layer into an aqueous solution containing 25 mM zinc nitrate and 25 mM methenamine at 92 °C for 24 h. The as-grown nanowire arrays were then annealed at 400 °C for 30 min in the tube-furnace to remove the impurities, improve the crystalline and reduce the interfacial defects [29,30].

The prepared ZnO nanowire arrays acted as the foundation of the subsequent core-shell structure followed by a series of successive ion-replacement process with hydrothermal method. Se powder and $NaBH_4$ were mixed in deionized water to prepare 6 mM Se^{2-} aqueous solution when Se powder was completely dissolved. ZnO/ZnSe arrays were formed by immersing the grown ZnO nanowire arrays into this Se^{2-} solution at 55 °C for 1 h. Afterwards, the ZnO/ZnSe arrays were douched by deionized water and then transferred into 25 mM $Cd(NO_3)_2$ solution at 95 °C for 6 h to fabricate ZnO/ZnSe/CdSe arrays. Finally, ZnO/ZnSe/CdSe/Cu_{2-x}Se arrays were prepared by soaking ZnO/ZnSe/CdSe arrays into 2.5 mM $Cu(NO_3)_2$ aqueous solution at 75 °C for 15 s. The reactions for the formation of ZnSe, CdSe and Cu_{2-x}Se are given as the following [31,32]

$$ZnO + Se^{2-} + H_2O \rightarrow ZnSe + 2OH^- \quad (1)$$

$$ZnSe + Cd^{2+} \rightarrow CdSe + Zn^{2+} \quad (2)$$

$$CdSe + Cu^{2+} \rightarrow Cu_{2-x}Se + Cd^{2+} \quad (3)$$

2.3. Characterization

X-ray diffraction (XRD) measurements were recorded on a diffractometer XD-D1 (SHIMADZU, Japan) by using Cu Kα irradiation. The morphologies of products were characterized using a scanning electron microscope (SEM) S-4800 (HITACHI, Japan) and a transmission electron microscope (TEM) JEM-2100 (JEOL, Japan). The elemental component was measured by an energy dispersive spectrometer (EDS) E-MAX (HORIBA, France). The UV–vis absorption spectra were acquired by using a Lambda 950 UV/vis/NIR spectrophotometer (Perkin-Elmer, USA).

2.4. PEC measurements

The PEC measurements were evaluated in a bipotentiostat model AFCBP1 (PINE, USA) using a standard three-compartment cell under UV–vis light irradiation at 100 mW/cm^2 of a 300 W xenon lamp PLS-SXE300 (Perfect Light, China). An Ag/AgCl electrode and a Pt wire acted as the reference electrode and counter electrode, respectively. A mixed aqueous solution containing Na_2SO_3 (0.5 M) and Na_2S (0.5 M) was used as the electrolyte. The electrochemical impedance spectra (EIS) were obtained under the UV–vis light illu-

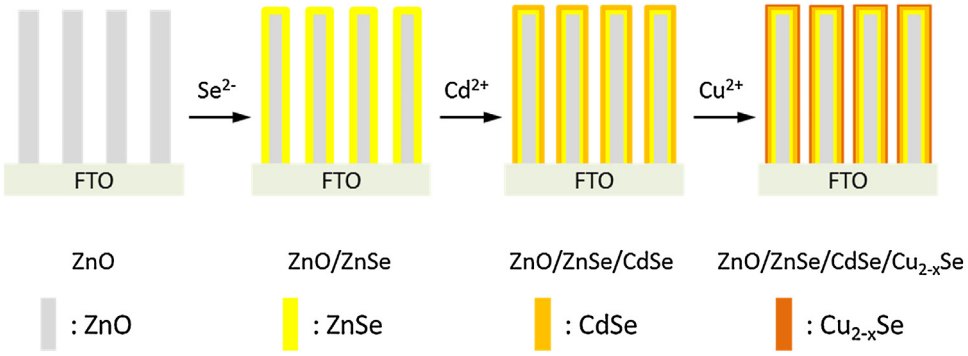

Fig. 1. Ion-replacement processes for ZnO/ZnSe, ZnO/CdSe, ZnO/ZnSe/CdSe and ZnO/ZnSe/CdSe/$Cu_{2-x}Se$ core–shell nanowire arrays.

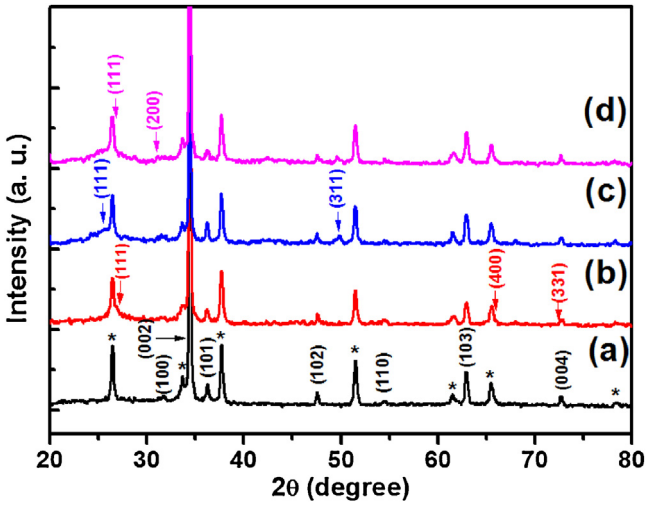

Fig. 2. XRD patterns of (a) ZnO, (b) ZnO/ZnSe, (c) ZnO/ZnSe/CdSe and (d) ZnO/ZnSe/CdSe/$Cu_{2-x}Se$ nanowire arrays.

mination of 100 mW/cm^2. An AC potential wave with open circuit voltage of 1–10^5 Hz and amplitude of 5 mV was applied to the PEC system of each sample.

A monochromator CS260-USB-Q-MC-A (Newport, USA) was used as the light source in order to study the wavelength-dependent photoresponse of the samples, and the area of the light beam on the samples was 1 cm^2. IPCE was calculated as following equation [33]

$$\mathrm{IPCE} = \frac{1240I\left(\mathrm{mA/cm^2}\right)}{\lambda\,(\mathrm{nm}) \times J_{\mathrm{light}}\left(\mathrm{mW/cm^2}\right)} \quad (4)$$

where I, λ and J_{light} were the photocurrent densities, the wavelength of the monochromatic light and the monochromatic light intensity, respectively.

3. Results and discussion

3.1. Characterization

Fig. 2 presented the XRD patterns for these samples. The diffraction peaks of the FTO glass were indicated with asterisk. The diffraction peaks of ZnO sample (Fig. 2a) matched well with ZnO in hexagonal phase (JPCDS 36-1451). It was obvious that the diffraction peak of ZnO (002) was much stronger than other peaks. This sharp diffraction peak (002) demonstrated that ZnO nanowire arrays were preferentially oriented in the *c*-axis direction [34], which was attributed to the annealing process. A layer of ZnSe appeared at the surface of the ZnO nanowires after immersing into Se^{2-}. The relevant new peaks appearing at 2theta of 27.224°, 65.858° and 72.632° in Fig. 2b were indexed to cubic ZnSe (JPCDS 37-1463). The subsequent ion-replacement reaction in Cd^{2+} solution brought out CdSe layer fabricated on the surface of ZnO/ZnSe nanowires, which was taken place by displacing part of Zn^{2+} by Cd^{2+}. The diffraction peaks developing at 2theta of 25.479° and 49.956° presented in Fig. 2c correspond to cubic CdSe (JPCDS 65-2891). The further ion-replacement process in Cu^{2+} solution took the final $Cu_{2-x}Se$ layer being established outside the ZnO/ZnSe/CdSe nanowires. The diffraction peaks emerging at 2theta of 26.749° and 31.026° in Fig. 2d amounted to berzelianite $Cu_{2-x}Se$ (JPCDS 06-0680). It is noteworthy that the diffraction peaks of ZnSe, CdSe and $Cu_{2-x}Se$ became broadened, which declared to be composed of nanocrystals.

Fig. 3 displayed the SEM images of the nanowire arrays grown in sequence on FTO glass. The lateral-view SEM for ZnO nanowire arrays clear demonstrated that ZnO nanowires were perpendicularly grown on FTO glass neatly, and the length of the nanowire was about 2–3 μm (Fig. 3a). The typical top-view SEM images of the nanowire arrays grown in sequence on FTO glass were shown in Fig. 3b–f, while the inset graphs were the homologous samples in high resolution. It was obvious that all the samples were perpendicularly aligned grown on FTO glass extremely neatly. Fig. 3b presented that ZnO nanowire arrays were regular hexagonal prisms, and the diameter of the cross section was about 50–200 nm. Both the top and lateral surfaces were flat and smooth with distinct edges. After being immersed in Se^{2-} solution, the top surfaces of ZnO/ZnSe nanowire arrays turned smooth as shown in Fig. 3c. Fig. 3d–f displayed ZnO/CdSe, ZnO/ZnSe/CdSe and ZnO/ZnSe/CdSe/$Cu_{2-x}Se$ nanowire arrays in sequence. It was quite clear that the nanowires grew bigger, the edges became less smooth, and the adjacent nanowires came to merge together. All these changes illustrated that the ion-replacement process resulted in the formation of new phases. The inset graphs in Fig. 3c–f revealed that the top surface of ZnO/ZnSe, ZnO/CdSe, ZnO/ZnSe/CdSe and ZnO/ZnSe/CdSe/$Cu_{2-x}Se$ were layered, which further indicated the ion-replacement process was achieved. The EDS analysis of ZnO/ZnSe/CdSe/$Cu_{2-x}Se$ in Fig. 4 showed O, Zn, Se, Cd and Cu co-existed. It was hard to calculate the x in $Cu_{2-x}Se$ because of the uncertain factor in analysis and computing process. For the achieved ZnO/ZnSe/CdSe/$Cu_{2-x}Se$ nanowire arrays, the proportion of every component in this quaternary ZnO/ZnSe/CdSe/$Cu_{2-x}Se$ nanowire arrays was evaluated by EDS spectra. The calculated contents are 77.86, 5.93, 5.78 and 10.43% for ZnO, ZnSe, CdSe and $Cu_{2-x}Se$, respectively.

Fig. 5 exhibited TEM images of ZnO/ZnSe, ZnO/ZnSe/CdSe and ZnO/ZnSe/CdSe/$Cu_{2-x}Se$ nanowires, demonstrating that all samples are core-shell structures with the core of ZnO. The shell was composed of dense nanoparticles, which agreed with the SEM images. The thickness of the shell of ZnO/ZnSe, ZnO/ZnSe/CdSe

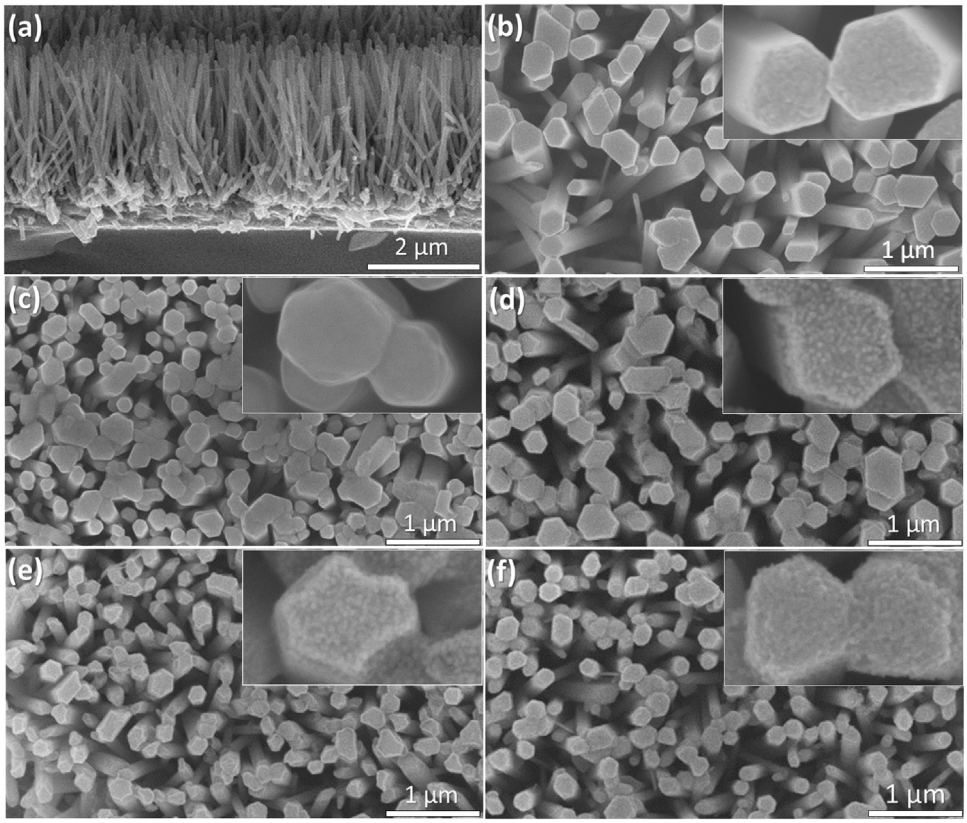

Fig. 3. (a) Lateral-view SEM image of ZnO nanowire arrays, and top-view SEM images of (b) ZnO, (c) ZnO/ZnSe, (d) ZnO/CdSe, (e) ZnO/ZnSe/CdSe and (f) ZnO/ZnSe/CdSe/$Cu_{2-x}Se$ nanowire arrays.

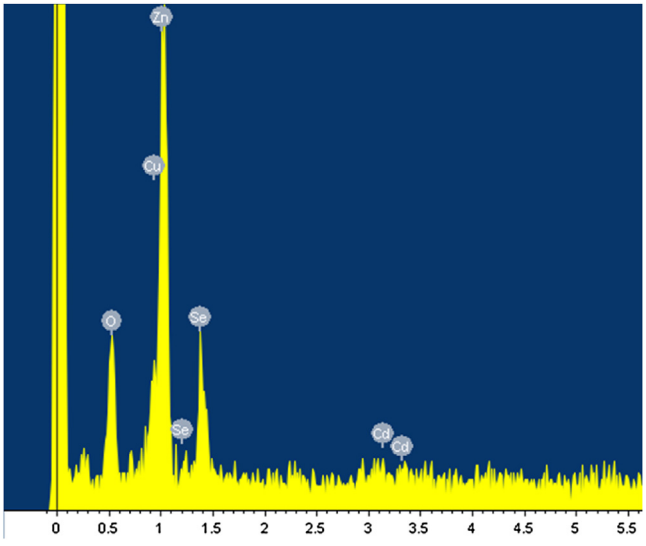

Fig. 4. EDS analysis for ZnO/ZnSe/CdSe/$Cu_{2-x}Se$ nanowire arrays.

and ZnO/ZnSe/CdSe/$Cu_{2-x}Se$ was 5.92 nm, 10.97 nm and 16.35 nm, respectively. The gradual increase of shell thickness confirms the generation of new phases. In ZnO/ZnSe nanowire, an obvious ZnO core and distinct ZnSe shell are observed as shown in Fig. 5a. The shell of ZnO/ZnSe/CdSe nanowire becomes slightly unclear and is composed of nanoparticles as presented in Fig. 5b. Fig. 5c shows that the shell of ZnO/ZnSe/CdSe/$Cu_{2-x}Se$ nanowire becomes rough and also is composed of nanoparticles.

Fig. 6 showed the UV–vis absorption spectra of ZnO, ZnO/ZnSe, ZnO/ZnSe/CdSe and ZnO/ZnSe/CdSe/$Cu_{2-x}Se$ nanowire arrays. The inset graph was the optical image of these samples. ZnO nanowire arrays grown on FTO glass showed strong UV absorption but scarcely any absorption in the visible light region, which agreed with the white color. The absorption edge was about 375 nm and matched well with the band gap at 3.3 eV [35]. After being immersed in Se^{2-} solution, ZnO/ZnSe got yellow in color, which agreed with the absorption of part of visible light. The absorption shoulder at 459 nm was in accordance with the band gap (2.7 eV) of ZnSe. There was an absorption tail extending into the longer wavelength (i.e, lower photon energy), which was due to the defect states [36]. In addition, it has been reported that the indirect band gap of coaxial nanowires with type-II heterostructures over two wide-bandgap semiconductors would be narrower than either of the semiconductors [37]. Furthermore, the porous surfaces of ZnSe layer enhanced the specific surface area, which improved the absorption of incident light. ZnO/ZnSe/CdSe turned orange followed by ion-replacement process of Cd^{2+}, and the absorption edge shifted to 730 nm in wavelength, accorded with the band gap (1.7 eV) of CdSe. The final product ZnO/ZnSe/CdSe/$Cu_{2-x}Se$ came into brown in color, and this further changed to the darker color, implying that the absorption edge extended further to near infrared region. All these demonstrated that UV–vis absorption was enhanced by the formation of ZnSe, CdSe and $Cu_{2-x}Se$ successively during ion-replacement process.

3.2. PEC performance

Fig. 7 displayed the UV–vis light responses and photocurrent densities of the ZnO, ZnO/ZnSe, ZnO/CdSe, ZnO/ZnSe/CdSe and ZnO/ZnSe/CdSe/$Cu_{2-x}Se$ electrodes, with the bias voltage of 0 V versus Ag/AgCl. The photocurrent of each sample rose to the peak value rapidly as soon as the simulated solar illumination

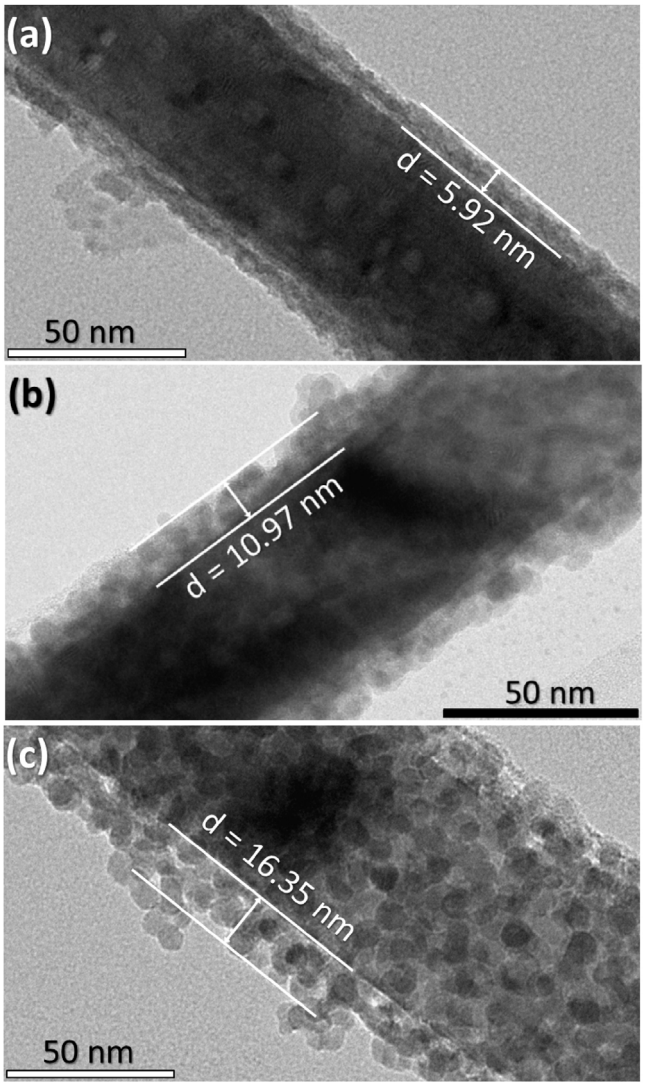

Fig. 5. TEM images for (a) ZnO/ZnSe, (b) ZnO/ZnSe/CdSe and (c) ZnO/ZnSe/CdSe/$Cu_{2-x}Se$ nanowires.

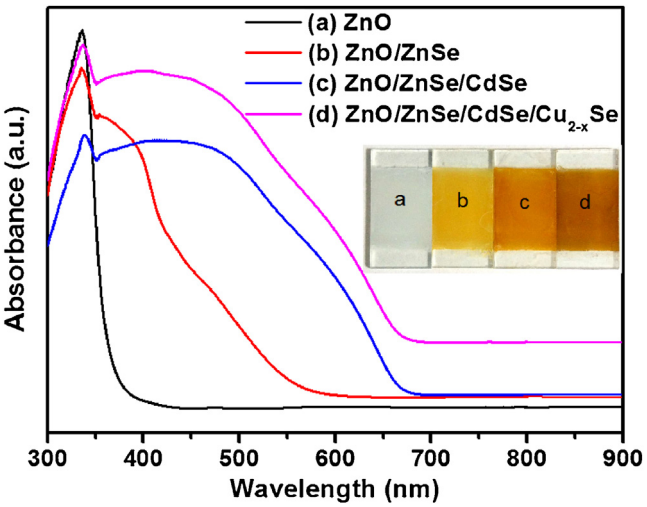

Fig. 6. UV–vis absorption spectra of ZnO, ZnO/ZnSe, ZnO/ZnSe/CdSe and ZnO/ZnSe/CdSe/$Cu_{2-x}Se$ nanowire arrays.

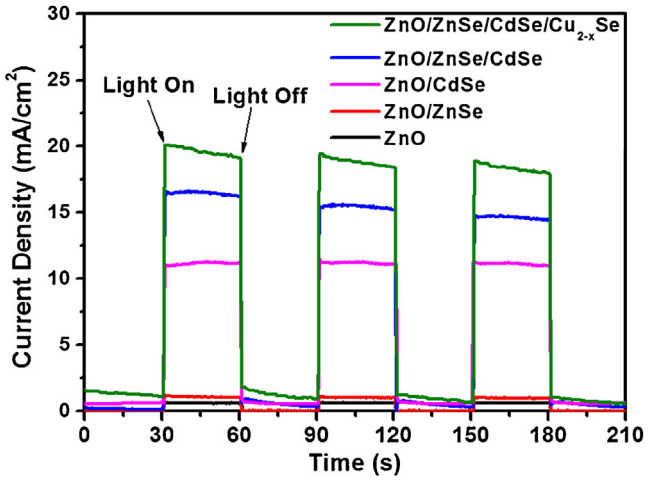

Fig. 7. UV–vis light responses and photocurrent densities of ZnO, ZnO/ZnSe, ZnO/CdSe, ZnO/ZnSe/CdSe and ZnO/ZnSe/CdSe/$Cu_{2-x}Se$ electrodes.

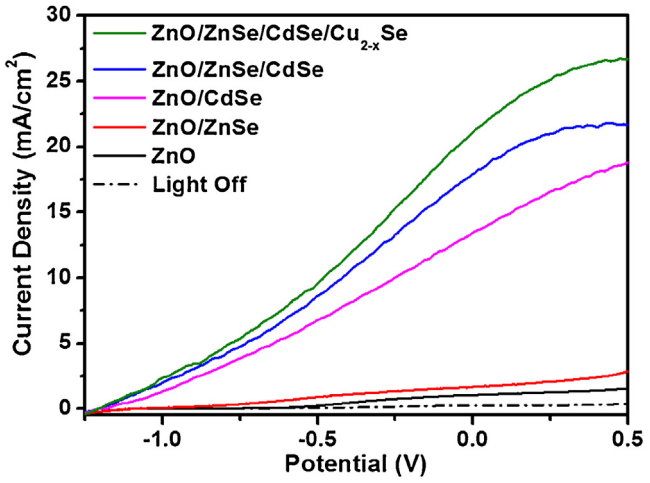

Fig. 8. LSV curves of ZnO, ZnO/ZnSe, ZnO/ZnSe/CdSe, ZnO/CdSe and ZnO/ZnSe/CdSe/$Cu_{2-x}Se$ electrodes.

was turned on. Thereafter it declined gradually to reach a steady state. The decay time of each electrode extended successively, and this was correlative to the lifetime of the photo-induced carriers in revenant electrode [38]. The photocurrent density of the ZnO electrode was 0.70 mA/cm^2. The ZnSe converted from a portion of ZnO in the ZnO/ZnSe nanowire arrays enhanced the photocurrent to 1.24 mA/cm^2 attributed to the improved visible light absorption. The photocurrent density of ZnO/CdSe electrode was 11.55 mA/cm^2. The formation of CdSe layer on ZnO/ZnSe/CdSe nanowire arrays generated a conspicuous growth to 16.65 mA/cm^2 in photocurrent density. This remarkable improvement was due to the formation of CdSe layer, which agreed with the increased visible light absorption. The photocurrent densities of the final product of ZnO/ZnSe/CdSe/$Cu_{2-x}Se$ nanowire arrays reached 20.57 mA/cm^2, which was 29.4 times higher than that of the original ZnO nanowire arrays. The improved photocurrent densities along with the formation of every layer got involved to the consecutive improvement of the PEC performance.

The linear sweep voltammograms (LSVs) were measured to investigate the correlation between UV–vis light photocurrent densities and bias voltage. The LSV curves were shown in Fig. 8 obtained at the bias voltage from −1.25 V to 0.5 V. All electrodes exhibited improvement in photocurrent densities along with the bias voltage increase. ZnO electrode exhibited low photocurrent density as the

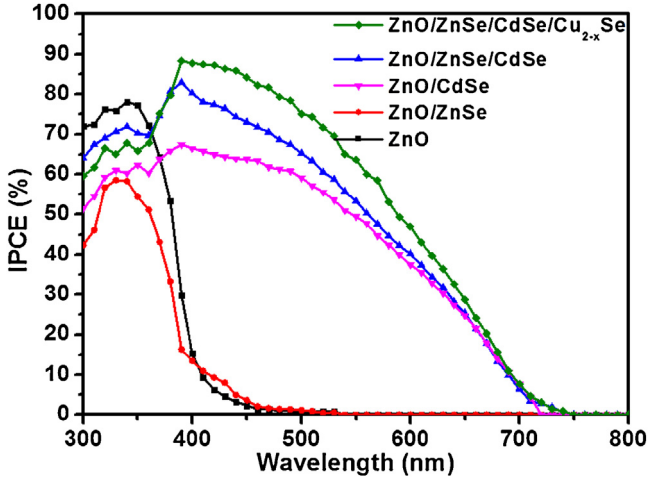

Fig. 9. IPCE curves of ZnO, ZnO/ZnSe, ZnO/CdSe, ZnO/ZnSe/CdSe and ZnO/ZnSe/CdSe/$Cu_{2-x}Se$ electrodes.

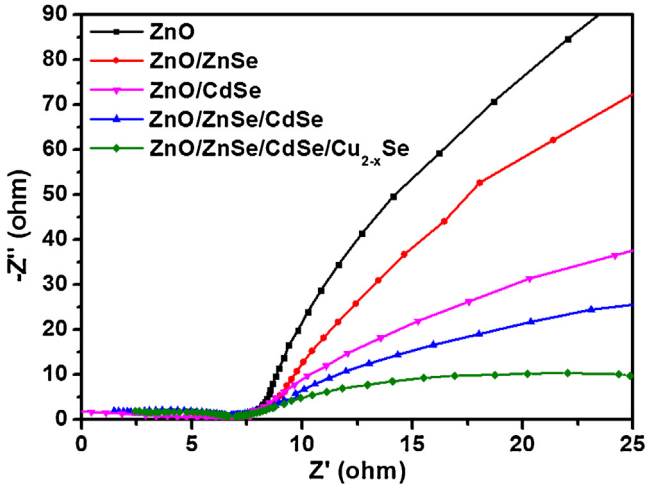

Fig. 10. EIS curves of ZnO, ZnO/ZnSe, ZnO/CdSe, ZnO/ZnSe/CdSe and ZnO/ZnSe/CdSe/$Cu_{2-x}Se$ electrodes.

bias voltage increase. There is limited improvement in photocurrent density for the ZnO/ZnSe electrode. The formation of CdSe and $Cu_{2-x}Se$ improved the photocurrent densities significantly, which was attributed to the enhanced visible light absorption and the efficient separation of photogenerated electrons and holes in achieved heterogeneous photocatalyst [39,28].

The IPCE measurements were performed on ZnO, ZnO/ZnSe, ZnO/CdSe, ZnO/ZnSe/CdSe and ZnO/ZnSe/CdSe/$Cu_{2-x}Se$ samples without bias potential versus Ag/AgCl, in order to quantify the photoelectric conversion efficiency of these samples in illumination of disparate wavelength. The IPCE curves for these five samples were exhibited in Fig. 9. The photoresponse of ZnO sample was almost exclusively active in the UV region, while the ZnO/ZnSe sample extended its photoresponse to the visible light region, which agreed with the respective UV–vis absorption. The photoresponse region of the ZnO/ZnSe/CdSe sample substantially increased to more than 700 nm, which matched well with the UV–vis spectrum. Furthermore, the IPCE enhanced significantly in visible light region. On one hand, the heterojunction of CdSe layer contributed excellent absorbance in visible light region attributed to the narrow band gap. On the other hand, the multiple exciton generation effect of CdSe resulted in an enhanced absorption in the visible light region due to the producing of multiple excitons (i.e, electron–hole pairs) generated by each absorbed high-energy photon [40]. The synergistic action effectively improved both the photon utilization and the exciton productivity. A slight increasement of the photoresponse in the visible light region occurred in ZnO/ZnSe/CdSe/$Cu_{2-x}Se$ sample, contrasted with the ZnO/ZnSe/CdSe sample. Moreover, the IPCE in visible light region enhanced. IPCE reached the maximum of 87.6% at the wavelength of 410 nm, and kept higher than 50% within the wavelength range from 300 to 590 nm. $Cu_{2-x}Se$ layer in ZnO/ZnSe/CdSe/$Cu_{2-x}Se$ nanowire arrays played the role as the hole mediator over the surface of CdSe, facilitating the holes transmitting between the interface of the semiconductor and electrolyte [41]. Moreover, the p-type $Cu_{2-x}Se$ formed p-n junctions over the CdSe layer, which raised the efficiency of the separation and transportation of the photo-induced carriers. It was worth noting that the IPCE values in the vicinity of the infrared region of the ZnO/ZnSe/CdSe/$Cu_{2-x}Se$ sample was approximates to zero, which was in contrast with the infrared absorbance recorded in the UV–vis absorption spectrum data. This was attributed to the strong infrared absorption of water as the solvent in the electrolyte. The growth in succession of the IPCE for these samples benefited from the combined effect of these factors above, which contributed to the remarkable increasement of the photocurrent densities.

3.3. Mechanism

The EIS curves were performed to investigate the electrochemical reaction kinetics of ZnO, ZnO/ZnSe, ZnO/CdSe, ZnO/ZnSe/CdSe and ZnO/ZnSe/CdSe/$Cu_{2-x}Se$ electrodes. Fig. 10 displayed EIS curves scanned from 1 to 10^5 Hz under simulated sunlight. The diameter of the semi-circle arc in each EIS curve was relevant to electrochemical reaction kinetics. A shorter diameter was associated with a smaller charge transfer resistance, while the charge transfer resistance was related to the recombination of photo-induced electron-hole pairs. Therefore, the diameter of semi-circle arc was negatively correlated to the efficiency of separation and transportation of photo-generated carries corresponded to each electrode [42,43]. As shown in Fig. 10, the diameter of the semi-circle arc in EIS curves of ZnO, ZnO/ZnSe, ZnO/CdSe, ZnO/ZnSe/CdSe and ZnO/ZnSe/CdSe/$Cu_{2-x}Se$ electrodes shortened successively, indicating the gradually increasing efficiency of charge separation and transportation. These EIS results conformed to the improvement of the PEC properties, which were due to the formation of heterostructures during the ion-replacement process.

Photo-generated charge carriers were separated under the illumination in semiconductor. The electrons excited by incident light jumped to the conduction band (CB), while the holes left in the valence band (VB). The excited electrons in the heterojunction structures transported from the CB with more negative potential to the CB with less negative potential. In the same way, the holes transmitted from the VB with more positive potential to the VB with less positive potential [44]. The separation and transportation of photo-induced carriers in ZnO/ZnSe/CdSe/$Cu_{2-x}Se$ nanowire arrays were declared in Fig. 11. Fig. 11 indicated the relative positions of the energy levels corresponded with each layer in ZnO/ZnSe/CdSe/$Cu_{2-x}Se$ core–shell nanowire arrays. It was clear that the photo-induced electrons in $Cu_{2-x}Se$ layer firstly flowed to the CB of CdSe, then the electrons from the CB of CdSe and ZnSe layers transferred together to the CB of ZnO core. After that, the collected excited electrons were transported through the conductive FTO glass and the external circuit in sequence, and finally arrived at the Pt wire, which served as the counter electrode during decomposing the water to produce hydrogen. Similarly, the holes in both ZnSe and CdSe layers flowed to the VB of $Cu_{2-x}Se$ layer, and then reacted with the sacrificial agent in the electrolyte consisting of Na_2S and Na_2SO_3. The appropriate potential differences of CB and VB in each layer of ZnO/ZnSe/CdSe/$Cu_{2-x}Se$ core–shell nanowire

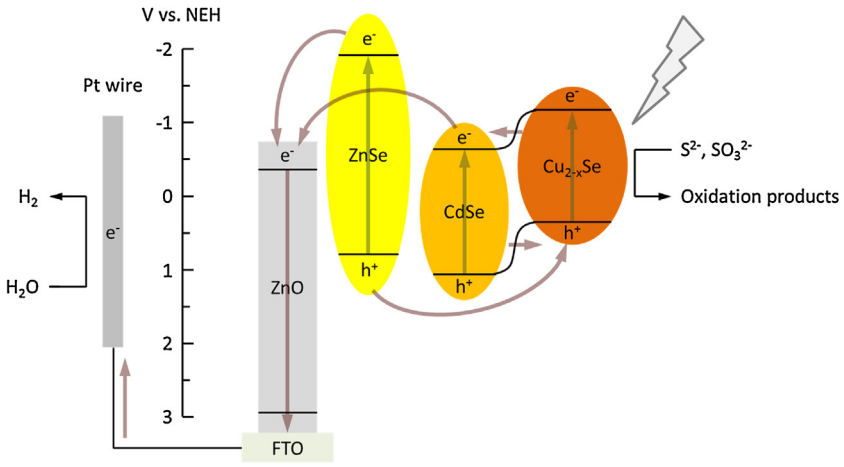

Fig. 11. Separation and transportation process for the photo-generated electron-hole pairs in ZnO/ZnSe/CdSe/$Cu_{2-x}Se$ nanowire arrays.

arrays offered fluent and efficient transportation of photo-induced carriers.

4. Conclusions

A facile ion-replacement method has been developed to design and fabricate ZnO/ZnSe/CdSe/$Cu_{2-x}Se$ core–shell nanowire arrays. By efficiently synergistic effects of materials, the fabricated ZnO/ZnSe/CdSe/$Cu_{2-x}Se$ core–shell nanowire arrays exhibit superior PEC performance with the highest photocurrent density of 20.57 mA/cm^2 at 0 V versus Ag/AgCl under illumination with AM 1.5G, which is 29.4 times higher than that of the ZnO nanowire arrays. More importantly, the IPCE value of the designed ZnO/ZnSe/CdSe/$Cu_{2-x}Se$ core–shell nanowire arrays reaches up to 87.6% at 410 nm without applying bias potential. In this core-shell structure, core ZnO nanowire arrays provided large specific area and electron access along the axial direction. The ZnSe layer further extended specific surface area and improved the incident light absorptivity. The narrow-bandgap CdSe layer enhanced the visible light absorption vastly and fully utilized the incident light. The outmost p-type $Cu_{2-x}Se$ layer coupled with n-type CdSe layer to form p-n junctions, which not only prevent the recombination, but also promote the efficient separation and transmission of photo-excited electron-hole pairs. The highly synergistic actions of each component in ZnO/ZnSe/CdSe/$Cu_{2-x}Se$ core–shell nanowire arrays make electrode to achieve superior PEC performance. The synthetic strategy achieved in this work has promising applications for designing highly efficient electrodes of other materials for water splitting.

Acknowledgment

This research was supported by the National Natural Science Foundation of China (Grant Nos. 51132002, 51372282, 51072024, 11074312, 11374377, 11474174, 61575225 and 11404414).

References

[1] J. Zhu, F. Fan, R. Chen, H. An, Z. Feng, C. Li, Direct imaging of highly anisotropic photogenerated charge separations on different facets of a single $BiVO_4$ photocatalyst, Angew. Chem. 127 (2015) 9239–9242.
[2] T. Kamegawa, S. Matsuura, H. Seto, H. Yamashita, A visible-light-harvesting assembly with a sulfocalixarene linker between dyes and a Pt-TiO_2 photocatalyst, Angew. Chem. Int. Ed. 52 (2013) 916–919.
[3] H. Dotan, K. Sivula, M. Grätzel, A. Rothschild, S.C. Warren, Probing the photoelectrochemical properties of hematite (α-Fe_2O_3) electrodes using hydrogen peroxide as a hole scavenger, Energy Environ. Sci. 4 (2011) 958–964.
[4] C. Han, M.Q. Yang, B. Weng, Y.J. Xu, Improving the photocatalytic activity and anti-photocorrosion of semiconductor ZnO by coupling with versatile carbon, Phys. Chem. Chem. Phys. 16 (2014) 16891–16903.
[5] A. Nezamzadeh-Ejhieh, M. Karimi-Shamsabadi, Comparison of photocatalytic efficiency of supported CuO onto micro and nano particles of zeolite X in photodecolorization of methylene blue and methyl orange aqueous mixture, Appl. Catal. A: Gen. 477 (2014) 83–92.
[6] Q. Wang, T. Hisatomi, S.S.K. Ma, Y. Li, K. Domen, Core/shell structured La-and Rh-codoped $SrTiO_3$ as a hydrogen evolution photocatalyst in Z-scheme overall water splitting under visible light irradiation, Chem. Mater. 26 (2014) 4144–4150.
[7] A. Tanaka, K. Hashimoto, H. Kominami, Visible-light-induced hydrogen and oxygen formation over Pt/Au/WO_3 photocatalyst utilizing two types of photoabsorption due to surface plasmon resonance and band-gap excitation, J. Am. Chem. Soc. 136 (2014) 586–589.
[8] F. Zhang, X. Li, Q. Zhao, A. Chen, Facile and controllable modification of 3D In_2O_3 microflowers with In_2S_3 nanoflakes for efficient photocatalytic degradation of gaseous ortho-dichlorobenzene, J. Phys. Chem. C 120 (2016) 19113–19123.
[9] J. Wang, Z. Wang, B. Huang, Y. Ma, Y. Liu, X. Qin, Y. Dai, Oxygen vacancy induced band-gap narrowing and enhanced visible light photocatalytic activity of ZnO, ACS Appl. Mater. Interface 4 (2012) 4024–4030.
[10] Y.K. Lim, E.W.K. Koh, Y.W. Zhang, H. Pan, Ab initio design of GaN-based photocatalyst: ZnO-codoped GaN nanotubes, J. Power Sources 232 (2013) 323–331.
[11] S.H. Ko, D. Lee, H.W. Kang, K.H. Nam, J.Y. Yeo, S.J. Hong, H.J. Sung, Nanoforest of hydrothermally grown hierarchical ZnO nanowires for a high efficiency dye-sensitized solar cell, Nano Lett. 11 (2011) 666–671.
[12] B. Qiu, M. Xing, J. Zhang, Mesoporous TiO_2 nanocrystals grown in situ on graphene aerogels for high photocatalysis and lithium-ion batteries, J. Am. Chem. Soc. 136 (2014) 5852–5855.
[13] W. Zhou, Z. Yin, Y. Du, X. Huang, Z. Zeng, Z. Fan, H. Zhang, Synthesis of few-layer MoS_2 nanosheet-coated TiO_2 nanobelt heterostructures for enhanced photocatalytic activities, Small 9 (2013) 140–147.
[14] S. Khanchandani, S. Kumar, A.K. Ganguli, Comparative study of TiO_2/CuS core/shell and composite nanostructures for efficient visible light photocatalysis, ACS Sustain. Chem. Eng. 4 (2016) 1487–1499.
[15] K. Ullah, L. Zhu, S. Ye, S.B. Jo, W.C. Oh, Photocatalytic and reusability studies of novel ZnSe/graphene nanocomposites synthesized via one pot hydrothermal techniques, Asian J. Chem. 26 (2014) 4097.
[16] A.R. Khataee, M. Hosseini, Y. Hanifehpour, M. Safarpour, S.W. Joo, Hydrothermal synthesis and characterization of Nd-doped ZnSe nanoparticles with enhanced visible light photocatalytic activity, Res. Chem. Intermed. 40 (2014) 495–508.
[17] M. Zhou, D. Han, X. Liu, C. Ma, H. Wang, Y. Tang, J. Yang, Enhanced visible light photocatalytic activity of alkaline earth metal ions-doped CdSe/rGO photocatalysts synthesized by hydrothermal method, Appl. Catal. B: Environ. 172 (2015) 174–184.
[18] P. Wang, D. Li, J. Chen, X. Zhang, J. Xian, X. Yang, Y. Shao, A novel and green method to synthesize CdSe quantum dots-modified TiO_2 and its enhanced visible light photocatalytic activity, Appl. Catal. B: Environ. 160 (2014) 217–226.
[19] C. Clavero, Plasmon-induced hot-electron generation at nanoparticle/metal-oxide interfaces for photovoltaic and photocatalytic devices, Nat. Photonics 8 (2014) 95–103.
[20] P. Fageria, S. Gangopadhyay, S. Pande, Synthesis of ZnO/Au and ZnO/Ag nanoparticles and their photocatalytic application using UV and visible light, RSC Adv. 4 (2014) 24962–24972.
[21] H. Zhou, A. Colli, A. Ahnood, Y. Yang, N. Rupesinghe, T. Butler, G.A. Amaratunga, Arrays of parallel connected coaxial multiwall-carbon-nanotube–amorphous-silicon solar cells, Adv. Mater. 21 (2009) 3919–3923.

[22] W. Chen, N. Zhang, M.Y. Zhang, X.T. Zhang, H. Gao, J. Wen, Controllable growth of ZnO–ZnSe heterostructures for visible-light photocatalysis, CrystEngComm 16 (2014) 1201–1206.
[23] A.S. Khomane, P.P. Hankare, Structural: optical and electrical characterization of chemically deposited CdSe thin films, J. Alloy Compd. 489 (2010) 605–608.
[24] J. Ouyang, M. Chang, Y. Zhang, X. Li, CdSe-sensitized TiO_2 nanotube array film fabricated by ultrasonic-assisted electrochemical deposition and subsequently wrapped with TiO_2 thin layer for the visible light photoelectrocatalysis, Thin Solid Films 520 (2012) 2994–2999.
[25] S. Shen, L. Guo, X. Chen, F. Ren, S.S. Mao, Effect of Ag_2S on solar-driven photocatalytic hydrogen evolution of nanostructured CdS, Int. J. Hydrogen Energy 35 (2010) 7110–7115.
[26] X. Wang, K.L. Pey, C.H. Yip, E.A. Fitzgerald, D.A. Antoniadis, Vertically arrayed Si nanowire/nanorod-based core-shell pn junction solar cells, J. Appl. Phys. 108 (2010) 124303.
[27] J. Xu, X. Yang, Q.D. Yang, T.L. Wong, S.T. Lee, W.J. Zhang, C.S. Lee, Arrays of CdSe sensitized ZnO/ZnSe nanocables for efficient solar cells with high open-circuit voltage, J. Mater. Chem. 22 (2012) 13374–13379.
[28] W.X. Ouyang, Y.X. Yu, W.D. Zhang, High and stable photoelectrochemical activity of ZnO/ZnSe/CdSe/Cu_xS core–shell nanowire arrays: nanoporous surface with Cu_xS as a hole mediator, Phys. Chem. Chem. Phys. 17 (2015) 14827–14835.
[29] M.H. Park, H.J. Kim, Y.J. Kim, W. Jeon, T. Moon, C.S. Hwang, Ferroelectric properties and switching endurance of $Hf_{0.5}Zr_{0.5}O_2$ films on TiN bottom and TiN or RuO_2 top electrodes, Phys. Status Solidi R. 8 (2014) 532–535.
[30] P.Y. Yang, J.L. Wang, W.C. Tsai, S.J. Wang, J.C. Lin, I.C. Lee, H.C. Cheng, Effect of oxygen annealing on the ultraviolet photoresponse of p-NiO-nanoflower/n-ZnO-nanowire heterostructures, J. Nanosci. Nanotechnol. 11 (2011) 5737–5743.
[31] B. Wang, T. Liu, C. Xia, F. Zhou, F. He, R. Liu, H. Wang, The structure and photovoltaic properties of double-shell TiO_2/ZnSe/CdSe nanocable arrays synthesized by using TiO_2/ZnO nanocables template, Mater. Res. Bull. 59 (2014) 234–240.
[32] Y. Zhang, Y. Shen, X. Wang, L. Zhu, B. Han, L. Ge, A. Xie, Enhancement of blue fluorescence on the ZnSe quantum dots doped with transition metal ions, Mater. Lett. 78 (2012) 35–38.
[33] G. Liu, L.C. Yin, J. Wang, P. Niu, C. Zhen, Y. Xie, H.M. Cheng, A red anatase TiO_2 photocatalyst for solar energy conversion, Energy Environ. Sci. 5 (2012) 9603–9610.
[34] M.F. Malek, M.H. Mamat, Z. Khusaimi, M.Z. Sahdan, M.Z. Musa, A.R. Zainun, M. Rusop, Sonicated sol–gel preparation of nanoparticulate ZnO thin films with various deposition speeds: the highly preferred c-axis (002) orientation enhances the final properties, J. Alloy Compd. 582 (2014) 12–21.
[35] S.M. Hatch, J. Briscoe, S. Dunn, A self-powered ZnO-nanorod/CuSCN UV photodetector exhibiting rapid response, Adv. Mater. 25 (2013) 867–871.
[36] F. Liu, M.H. Jang, H.D. Ha, J.H. Kim, Y.H. Cho, T.S. Seo, Facile synthetic method for pristine graphene quantum dots and graphene oxide quantum dots: origin of blue and green luminescence, Adv. Mater. 25 (2013) 3657–3662.
[37] Z. Wu, Y. Zhang, J. Zheng, X. Lin, X. Chen, B. Huang, J. Kang, An all-inorganic type-II heterojunction array with nearly full solar spectral response based on ZnO/ZnSe core/shell nanowires, J. Mater. Chem. 21 (2011) 6020–6026.
[38] C.X. Guo, Y. Dong, H.B. Yang, C.M. Li, Graphene quantum dots as a green sensitizer to functionalize ZnO nanowire arrays on F-doped SnO_2 glass for enhanced photoelectrochemical water splitting, Adv. Energy Mater. 3 (2013) 997–1003.
[39] G. Sfyri, S. Sfaelou, K.S. Andrikopoulos, N. Balis, G.A. Voyiatzis, P. Lianos, Composite ZnSe-CdSe quantum dot sensitizers of solid-state solar cells and the beneficial effect of added Na_2S, J. Phys. Chem. C 118 (2014) 16547–16551.
[40] D. Esparza, I. Zarazuía, T. Loípez-Luke, A. Cerdaín-Pasaraín, A. Sánchez-Solís, A. Torres-Castro, E. De la Rosa, Effect of different sensitization technique on the photoconversion efficiency of CdS quantum dot and CdSe quantum rod sensitized TiO_2 solar cells, J. Phys. Chem. C 119 (2015) 13394–13403.
[41] J.G. Radich, N.R. Peeples, P.K. Santra, P.V. Kamat, Charge transfer mediation through Cu x S. The hole story of CdSe in polysulfide, J. Phys. Chem. C 118 (2014) 16463–16471.
[42] S.K. Balasingam, J.S. Lee, Y. Jun, Few-layered $MoSe_2$ nanosheets as an advanced electrode material for supercapacitors, Dalton Trans. 44 (2015) 15491–15498.
[43] X. Wang, C. Hu, H. Liu, G. Du, X. He, Y. Xi, Synthesis of CuO nanostructures and their application for nonenzymatic glucose sensing, Sens. Actuators B: Chem. 144 (2010) 220–225.
[44] S.J. Hong, S. Lee, J.S. Jang, J.S. Lee, Heterojunction $BiVO_4$/WO_3 electrodes for enhanced photoactivity of water oxidation, Energy Environ. Sci. 4 (2011) 1781–1787.